An eBook on Thermodynamics

Chapter 2

Unfolding and Targeting Thermodynamics of the Sarcin Ricin Loop and its DNA Analog

Calliste Reiling[1]; Luis A Marky[1*]

[1]Department of Pharmaceutical Sciences, University of Nebraska Medical Center, 986025 Nebraska Medical Center, Omaha, Nebraska 68198-6025.

*[*]**Correspondence to: Luis A Marky,** Department of Pharmaceutical Sciences, University of Nebraska Medical Center, 986025 Nebraska Medical Center, Omaha, Nebraska 68198-6025.*

Email: lmarky@unmc.edu

Abstract

The Sarcin Ricin Loop (SRL) is an important structure in rRNA involved in translation by interacting with elongation factors. However, SRL is susceptible to cleavage by the binding of toxic proteins, inhibiting translation. The aim of this work is to determine the thermodynamic contributions of a RNA/DNA targeting reaction relative to a DNA/DNA reaction and to determine if DNA oligonucleotides can be used to mimic the targeting of RNA structures. We used a thermodynamic approach to study both SRL (***rSRL***) and its DNA analog (***dSRL***) and have shown, based on enthalpic contributions, these two molecules are forming a similar secondary structure. The ***rSRL***, however, is more stable, by 5.4 kcal/mol, due to its greater thermal stability by 14.3 °C and higher unfolding enthalpy by 20.8 kcalmol. The targeting of these SRLs was carried out using the same DNA partially complementary strand, which was designed to interact with the unpaired bases of the loop and stem. This DNA single strand is able to disrupt each SRL yielding duplex products with similar unfolding thermodynamic profiles. Overall, the disruption of the ***rSRL*** resulted in a less favorable free energy term, by 3.5 kcal/mol, in agreement with its higher stability. The main conclusion is a DNA targeting

strand can be used to gain a better understanding for the formation of a RNA/DNA hybrid duplex, which would be the resulting product of an *in vivo* targeting reaction. However, the higher stability of the RNA molecule yields a lower and favorable reaction free energy term. This can be overcome by targeting loops with a higher number of unpaired bases.

Marky LA

Keywords: Sarcin Ricin Loop; Intramolecular nucleic acid structures; Thermodynamics; Oligonucleotide targeting; Differential Scanning Calorimetry.

1. Introduction

The Sarcin Ricin Loop (SRL) is a highly conserved region found in the 23S ribosomal RNA and is critical for the binding of elongation factors for the process of translation [1]. There are at least five different GTPase factors, all with different functionality that bind to SRL [2], including EF-Tu and EF-G [1, 3–6]. These elongation factors act to protect the bases from chemical modifications. In rat, the binding of a toxic protein, sarcin, cleaves the phosphodiester bond between G4325 and A4326, which inhibits the elongation factors from binding [7]. Ricin depurinates A4324 also inhibiting the binding of GTPase factors which causes the elongation process to cease due to the complete inactivation of the ribosome [8]. It has been shown that a short oligonucleotide (~30 nt) mimicking the sarcin ricin loop has a similar structure as when within the ribosomal RNA and still binds to its elongation factors [9, 10]. The SRL structure has two important conserved motifs which include a bulged-G motif and a GAGA tetraloop [11–15]. The bulged-G motif forms a base-triplet that is flanked by non-Watson-Crick base-pairs which are followed by Watson-Crick base-pairs [16]. Both motifs are important for the binding of elongation factors and toxins, [1, 13, 16–18] and together form a very unique site for the interaction of these proteins.

The binding of these toxins inhibits translation from occurring, which ultimately kills the cell. Using this idea of inhibiting the ribosomal function, a previous study showed that short DNA oligonucleotides when microinjected into *Xenopus* oocytes can bind to SRL and completely inhibit translation [19]. This finding becomes very important when trying to control gene expression using oligonucleotides. In general, oligonucleotides show remarkable selectivity with the ability to discriminate target sequences which differ by only a base of off target sequences [20–22]. There are three main approaches for the use of oligonucleotides as modulators of gene expression: the antisense, antigene, and small interfering RNA strategies [22]. In the antisense strategy, a DNA oligonucleotide binds to messenger RNA (mRNA) or ribosomal RNA (rRNA), forming a RNA/DNA hybrid duplex that inhibits translation by blocking the assembly of the translation machinery or by inducing an RNase H mediated cleavage of their mRNA target [20]. One disadvantage is the continuous supply of the particular mRNA sequence; therefore, a constant supply of the targeting oligonucleotide is needed to control its expression. To overcome this limitation and have a greater control over gene expression, one

can target the rRNA inhibiting the binding of the ribosome to the mRNA. The ribosome will no longer be able to translate mRNA to form proteins, ultimately resulting in cell death. One advantage of controlling translation opposed to transcription is the DNA oligonucleotide only needs to cross the cellular membrane in order to bind to its target. If the chromosomal DNA were to be targeted, the oligonucleotide would need to cross both the cellular and nuclear membranes [23]. However, there is still the issue of the hydrophilic nature of DNA oligonucleotides. DNA single strands without a secondary structure are considered slightly more hydrophobic, increasing its ability to cross the cell and/or to interact with micellar polycations that can be used as the delivery system. Another disadvantage is the oligonucleotide in the cell can be quickly degraded by nucleases. Fortunately, using single strands with chemical modifications can slow down this process allowing the oligonucleotide time to reach its target.

From a thermodynamic point of view, successful control of gene expression depends on the effective binding of a DNA oligonucleotide sequence to its target with tight affinity and specificity. This is provided by using sequences of 15-20 bases in length when targeting gene transcripts [20]; strong specificity is conferred by hydrogen bonding in the formation of Watson-Crick base-pairs, while high affinity is provided by the large negative free energy upon formation of a duplex product; thereby, competing efficiently with the proteins involved in translation. In the successful targeting of nucleic acid secondary structures with complementary strands, the strand must be able to invade and disrupt the secondary structure forming a larger number of base-pair stacks in the duplex product. This is accomplished by targeting the unpaired bases of the loops in the secondary structure of the RNA molecule.

We have previously shown many DNA secondary structures can be targeted with partially complementary DNA strands [24-27]. One objective of this study is to determine if a RNA/DNA hybridization reaction is similar to a DNA/DNA reaction to gain important insights to the targeting process and reaction products. The goal is to determine to what extent one can use a DNA/DNA system to mimic the targeting of RNA structures, provided the RNA and DNA targets are forming similar secondary structures. Knowing that a relative short DNA oligonucleotide can disrupt translation within cells by targeting the SRL molecule, it makes it a perfect modeling system for this study because of its known biological significance [19]. In this work, we have determined unfolding thermodynamic profiles for both SRL and its DNA analog and have targeted each molecule with the same partially complementary DNA strand to form either a RNA/DNA hybrid duplex or a DNA/DNA duplex, both with a dangling end. The DSC unfolding results show that the *SRL* is thermodynamically more stable that its DNA counterpart (***dSRL***) while similar thermodynamic profiles are obtained for the formation of the RNA/DNA and DNA/DNA duplex products of these targeting reactions. In this case, our results indicate that in the targeting of RNA molecules one should take into account its higher stability, by 3-5 kcal/mol.

2. Materials and Methods

2.1. Materials

Oligonucleotides were synthesized and HPLC purified by Integrated DNA Technologies, and desalted by column chromatography using G-10 Sephadex exclusion chromatography. Sequences and their designations for this work are shown in **(Figure 1).** Oligonucleotide solution concentrations were determined at 260 nm and 90 ºC using an AVIV 14DS spectrophotometer (Lakewood, NJ) and the molar extinction coefficients: 293.4 $mM^{-1}\,cm^{-1}$ (***rSRL***), 288 $mM^{-1}\,cm^{-1}$ (***dSRL***), 158.1 $mM^{-1}\,cm^{-1}$ (*CS*), from here on the *SRL* is called ***rSRL*** to distinguish from the DNA analog. The molar extinction coefficients were obtained by extrapolation of the tabulated values for dimers and monomeric bases [28, 29], from 25 °C to 90 °C using procedures previously reported.[29, 30] Extinction coefficients for duplexes (not shown) were calculated by averaging the molar extinction coefficients of the complementary strands. Inorganic salts were reagent grade from Sigma and used without further purification. Measurements were made in 10 mM sodium phosphate with 100 mM NaCl at pH 7.0.

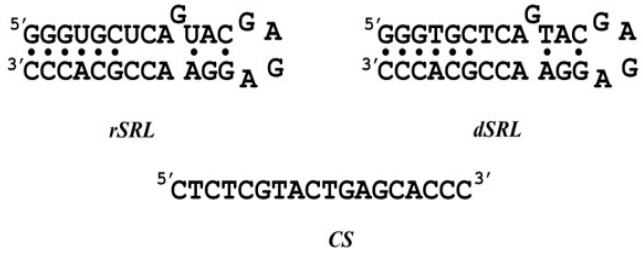

Figure 1: Sequences and Designations of Oligonucleotides.

2.2. Temperature-dependent UV Spectroscopy (UV melts)

Absorbance versus temperature profiles were measured at 260 nm with a thermoelectrically controlled AVIV Spectrophotometer Model 14DS UV-Vis. The temperature was scanned at a heating rate of ~0.6 °C/min, and shape analysis of the melting curves yielded T_Ms and van't Hoff enthalpies (ΔH_{VH}) [31]. The transition molecularity for the unfolding of a particular complex was obtained by monitoring the T_M as a function of strand concentration. Intramolecular complexes have T_Ms independent of strand concentration, while the T_Ms of intermolecular complexes varies with strand concentration [31].

2.3. Differential Scanning Calorimetry (DSC)

The total heat required for the unfolding of each oligonucleotide involved in the targeting reactions was measured with a VP-DSC from Malvern Panalytical. Standard thermodynamic profiles and transition temperatures, T_Ms, were obtained from DSC experiments using the following relationships [30, 31]: $\Delta H_{cal} = \int \Delta C_p(T)dT$; $\Delta S_{cal} = \int \Delta C_p(T)/TdT$, and the Gibbs equation, $\Delta G°_{(T)} = \Delta H_{cal} - T\Delta S_{cal}$, where ΔC_p is the anomalous heat capacity of the oligonucleotide solution during the unfolding process, ΔH_{cal} is the unfolding enthalpy, ΔS_{cal} is the unfolding entropy,

and $\Delta G^{\circ}_{(T)}$ is the unfolding free energy extrapolated to a common temperature assuming that both ΔH_{cal} and ΔS_{cal} terms are independent of temperature i.e., the unfolding of a nucleic acid is accompanied by a zeroth heat capacity effect [32, 33].

3. Results and Discussion

The overall experimental approach is as follows: First, we use DSC to determine the unfolding thermodynamics for ***rSRL*** and ***dSRL*** **(Figure 1).** Then, we use a DNA single strand of 18 bases long to target each structure; this single strand is complementary to the 14 bases of the top of the stems and the 4 unpaired bases of the loops. Each reaction was designed to yield favorable free energy contributions that are enthalpy driven. We use DSC to determine standard thermodynamic profiles for the unfolding of each reactant and product of these reactions, which are combined to generate Hess cycles, yielding thermodynamic profiles for each targeting reaction.

3.1. Unfolding thermodynamics of SRL and its DNA analog

(Figure 2A) shows typical UV melting curves for the helix-coil transition of ***rSRL*** *and* ***dSRL***; their sigmoidal behavior is characteristic of the temperature-induced unfolding of a nucleic acid oligonucleotide. Analysis of these curves yielded T_Ms and ΔH_{VHs} of 68°C, 50 kcal/mol (***rSRL***) and 55°C, 42 kcal/mol (***dSRL***), the higher thermal stability and unfolding enthalpy of ***rSRL*** is consistent with its higher hyperchromicity, by 6%, indicating higher base-pair stacking contributions. The T_M dependences on strand concentration are shown in **(Figure 2B)**, the T_Ms for both molecules remain the same over a tenfold change in total strand concentration. This shows both molecules are forming intramolecularly.

The DSC unfolding of each molecule is shown in **(Figure 2C)** and the resulting thermodynamic profiles are shown in **(Table 1).** Both molecules show single transitions, the ***rSRL*** transition is asymmetric while ***dSRL*** shows a symmetric transition, nevertheless, their DSC thermograms were fit with two transitions. We obtained for ***rSRL***, T_Ms of 61 and 69.1 °C, ΔH_{vH}s of 39 and 66 kcal/mol, ΔH_{cal}s of 48.3 and 41.6 kcal/mol, respectively, resulting in a total ΔH_{cal} of 89.9 kcal/mol. The ***dSRL*** transitions are characterized with similar parameters: T_M of 54.8 °C, ΔH_{vH} of 50 kcal/mol, and ΔH_{cal} of 69.1 kcal/mol. The overall results confirm the higher thermodynamic stability of ***rSRL*** due to higher base-pair stacking contributions, which is consistent with a higher unfolding enthalpy of 20.8 kcal. The lower values of the van't Hoff enthalpies, actually $\Delta H_{vH.}/\Delta H_{cal}$ ratios > 1, indicate the presence of intermediate states. Examination of the putative secondary structures of Figure 1, and going from left to right in their base pairing scheme, indicate 6 initial base-pairs (~5 base-pair stacks), followed by two weak mismatches: UC & CC (***rSRL***) or TC & CC (***dSRL***), a strong AA mismatch, a bulge G, a U•A or T•A base-pair, a strong AG mismatch, a C•G base-pair, and a terminal GAGA tetraloop. To determine their unfolding enthalpies using their corresponding nearest neighbor

contributions [34, 35], we have assumed that 8 base-pair stacks are contributing with the guanine as an extrahelical bulge **(Figure 1);** the additional three base-pair stacks correspond to stacking of the three pairs of bases at the end of the stem with the loop GA pair stack at the end of this stem. The calculation for these base-pair stacks is done as follows, for instance the UA/GA stack after the G bulge corresponds to the average N-N enthalpy of UA/UA and GA/AG. The overall exercise yielded N-N enthalpies of 97.5 kcal/mol (***rSRL***) and 67.8 kcal/mol (***dSRL***); if instead, we assumed the U, or T, to be the bulged bases instead of G and using the similar 8 base pair stacks, we obtained unfolding enthalpies of 99.8 kcal (***rSRL***) and 68.3 (***dSRL***). In summary, we estimate average enthalpies of 98.6 kacl/mol (***rSRL***) and 68.0 kcal (**dSR**L), which are in excellent agreement with their experimental values of 89.9 and 69.1 kcal, respectively. The higher enthalpy of the ***rSRL,*** by 20.8 kcal/mol, is consistent with the higher enthalpy of the average N-N RNA/RNA base-pair stack (10.9 kcal/mol) relative to the DNA/DNA base-pair stack (8.3 kcal/mol). This strongly suggests that the secondary structures of these two molecules are very similar. Furthermore, we have used the RNA and DNA N-N contributions [34, 35] to estimate the unfolding free energies for these molecules. This is done in a similar way as the enthalpy estimations with the inclusion of initiation free energies. We obtained unfolding Δ*G*s of 15.8 kcal/mol (***rSRL***) and 12.2 kcal/mol (***dSRL***), which are in good agreement with the experimental Δ*G*s of 15.9 kcal mol (***rSRL***) and 10.5 kcal/mol (***dSRL***). These values compare very well with the experimental free energies obtained earlier for a pair of DNA and RNA undecameric oligonucleotides, containing a total of 9 base-pair stacks: 14.0 kcal (RNA) and 9.3 kcal/mol (DNA) [36].

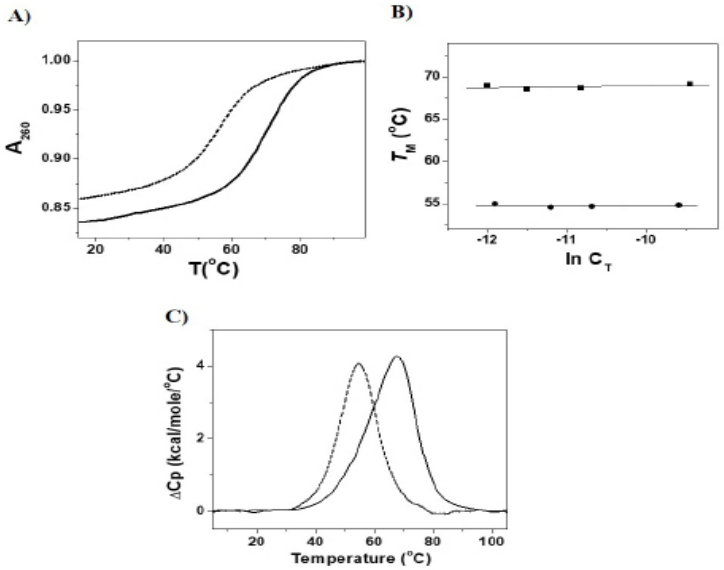

Figure 2: Temperature-unfolding curves of Sarcin Ricin Loop and DNA analog. (A) Normalized UV melting curves (~7 μM in total strands) for ***rSRL*** (—) and ***dSRL*** (- -). (B) Dependence of T_M on strand concentration: ***rSRL*** (●) and ***dSRL*** (■) (C) DSC curves (~70 μM) for ***rSRL*** (—) and ***dSRL*** (- -). Both UV and DSC experiments were carried out in 10 mM NaPi, 100 mM NaCl buffer at pH 7.0.

Table 1: Unfolding Thermodynamics for Sarcin Ricin Loop and its DNA analog.

Transition	T_M (°C)	ΔH (kcal/mol)	$T\Delta S$ (kcal/mol)	$\Delta G°_{(5)}$ (kcal/mol)
rSRL				
First	61.0	48.3	40.2	8.1
Second	69.1	41.6	33.8	7.8
		89.9	**74.0**	**15.9**
dSRL				
	54.8	**69.1**	**58.6**	**10.5**

All experiments were done in 10 mM sodium phosphate buffer and 100 mM NaCl at pH 7.0. Experimental errors are as follows: T_M (± 0.5 °C), ΔH (± 5 %), $T\Delta S$ (± 5 %), $\Delta G°_{(5)}$ (± 7%).

3.2. The *rSRL* is thermodynamically more stable than its DNA counterpart *dSRL*

The unfolding thermodynamic profiles of (**Table 1)** are plotted in **(Figure 3)** as folding thermodynamic parameters. The favorable free energy terms of the folding of each oligonucleotide results from a large compensation of a favorable enthalpy and unfavorable entropy contributions. Favorable enthalpy contributions include the formation of base pairs and base pair stacks while the ordering of a single-stranded oligonucleotide and the putative uptake of ions and water. Correspond to unfavorable entropy contributions. In this particular comparison the thermodynamic stability of ***rSRL*** is higher than ***dSRL***, by $\Delta\Delta G°$ = -5.4 kcal/mol, due to a favorable differential enthalpy ($\Delta\Delta H$ = -20.8 kcal/mol) and unfavorable differential entropy contributions ($\Delta(T\Delta S)$ = - 15.4kcal/mol). This is consistent with the average differential contribution of a single RNA base pair stack relative to a DNA base pair estimated from their respective N-N parameters: $\Delta\Delta G°$ = -0.9, $\Delta\Delta H$ = -2.6 and $\Delta(T\Delta S)$ = -1.7 kcal/mol. In summary, RNA is more stable thermodynamically due mainly to better base pair stacking contributions. Another factor to consider is RNA is less hydrated than DNA [36–38], i.e., it has less water to compete for hydrogen bonding with the bases. Therefore, the higher stability of RNA is an important factor to consider when designing oligonucleotides for the targeting of nucleic acids.

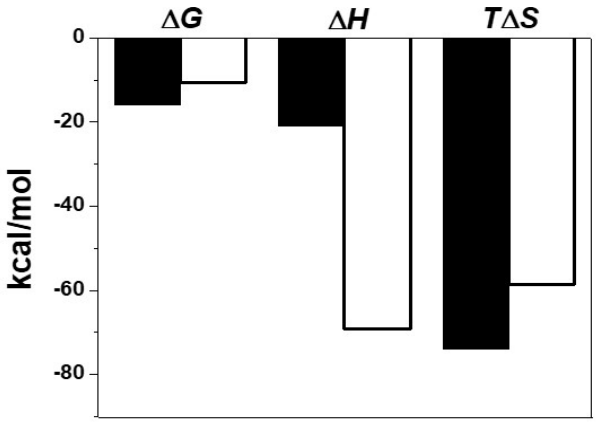

Figure 3: Comparison of unfolding thermodynamics: ***rSRL*** (solid bars) and ***dSRL*** (open bars) $\Delta\Delta G$ = -5.4, $\Delta\Delta H$ = -20.8 and $\Delta(T\Delta S)$ = -15.4 kcal/mol.

3.3. Targeting of the SRLs with a DNA complementary strand

We have designed a DNA single strand **(Figure 1)** that is complementary to the top stem and the four bases in the loop of ***rSRL*** and ***dSRL*** and investigated its reaction with each SRL, these targeting reactions are shown in **(Figure 4).** The experimental approach to determine thermodynamic profiles for each targeting reaction is to obtain DSC unfolding profiles of each reactant and resulting duplex product (with a dangling end). Then, we use this unfolding data to create thermodynamic Hess cycles corresponding to each targeting reaction. For comparative purposes, (**Figure 5A**) shows the DSC thermograms of ***rSRL***, **CS**, and the resulting ***RNA/DNA-Duplex***, while (**Figure 5B)** shows the DSC thermograms of ***dSRL***, ***CS***, and the ***DNA/DNA-Duplex***; standard thermodynamic profiles are listed in **(Table 2).** The unfolding of ***rSRL*** and ***dSRL***, have been discussed in a previous section. The DSC thermogram of ***CS*** shows a single transition with a total enthalpy of 18.5 kcal/mol, which is likely due to stacking contributions within the bases, especially with adjacent purine bases. The ***RNA/DNA-Duplex*** product of the first targeting reaction unfolds in a single asymmetric peak with a small shoulder ~ 63.9 °C and a well-defined transition temperature at 70.5 °C. This duplex unfolds with a total enthalpy of 147.6 kcal/mol; which is in excellent agreement with the unfolding enthalpy of 147.7 kcal/mol predicted using the RNA/DNA nearest-neighbor parameters.[39] On the other hand, the ***DNA/DNA-Duplex*** product of the second targeting reaction unfolds also in an asymmetric manner with a small shoulder at 63.4 °C, transition temperature of 68.5 °C, and total enthalpy of 139.4 kcal/mol, which is in agreement with a predicted enthalpy of 141.6 kcal/mol [39], obtained from the DNA N-N parameters. These results confirm that the partially complementary strand (***CS***) is able to invade and disrupt each SRL structure to form a duplex with a dangling end. The similarity of the enthalpy parameters for the folding of each duplex is due to the similar nearest-neighbor contributions of the RNA/DNA and DNA parameters, which is important to note when targeting RNA or DNA with a similar DNA complementary strand.

The Hess cycles profiles for these two targeting reactions, using the data of **(Table 2)**, are shown in the last two rows of Table 2. We obtained reaction enthalpies of 39.2 kcal/mol for the formation of ***RNA/DNA-Duplex*** and 51.8 kcal/mol for the formation of the ***DNA/DNA-Duplex***. The lower enthalpy value obtained with the targeting of ***rSRL*** is because of the higher initial energy needed to disrupt this molecule. Furthermore, using the N-N average enthalpies of a RNA/DNA base-pair stack and the average DNA base-pair stack, 8.8 and 8.3 kcal/mol respectively, we are estimating and additional formation of ~5 (***RNA/DNA-Duplex***) and ~6 (***DNA/DNA-Duplex***) base pair stacks in the duplex products of these two reactions. These additional stacking contributions correspond to the involvement of the unpaired bases of the loop, the weak mismatches, and the G bulge in the stem of the SRLs.

Reaction One:

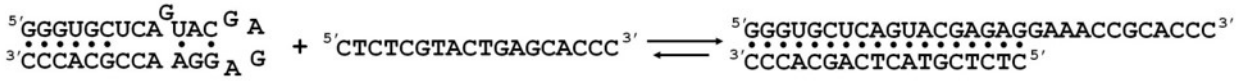

Reaction One:

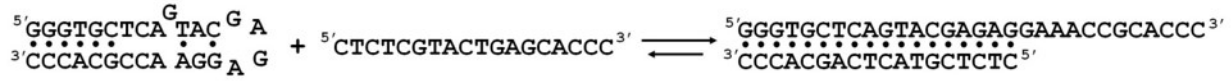

Figure 4: argeting Reactions of ***rSRL*** and ***dSRL*** with a DNA oligonucleotide yielding duplex products with a dangling end: RNA/DNA (Reaction 1) and DNA/DNA (Reaction 2).

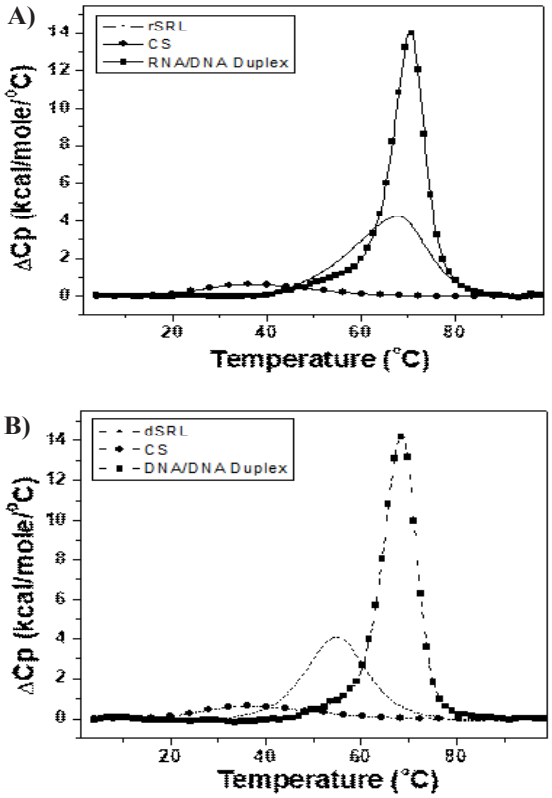

Figure 5: DSC unfolding curves for ***rSRL***, (66 µM), ***dSRL*** (69 µM), complementary strand (160 µM) and duplexes (30 µM) in 10 mM NaPi, 100 mM NaCl buffer at pH 7.0. (A) DSC curves of ***rSRL***, ***CS*** and ***RNA/DNA-Duplex*** (B) DSC curves of ***dSRL***, ***CS*** and ***DNA/DNA-Duplex***.

3.4. Comparison of RNA/DNA and DNA/DNA targeting reactions

The DSC targeting reactions were carried out at the same concentration of ***rSRL***/***dSRL*** and ***CS*** to form the same concentration of duplex to avoid any concentration dependence on the T_M. The two reaction products had very similar melting profiles with T_Ms and total enthalpies of 70.5 °C, 147.6 kcal/mol (***RNA/DNA-Duplex)***) and 68.5 °C, 139.4 kcal/mol (***DNA/DNA-Duplex***). Due to the agreement in T_M and enthalpy these duplexes have very similar thermodynamic stabilities i.e., free energies of -27.4 (***RNA/DNA-Duplex***) and -25.5 kcal/mol (***DNA/DNA-Duplex***), **(Table 2)**.

Overall, the favorable free energy term of each targeting reaction -9.5 and -13.0 kcal/mol resulted from a large compensation of a favorable enthalpy and unfavorable entropy

contributions **(Table 2 and Figure 6)**. The enthalpy contributions have been discussed extensively. Unfavorable entropy contributions include the bimolecular association of two strands and the putative immobilization of electrostricted water molecules and ions by the duplex product. In this particular thermodynamic comparison, the targeting of ***rSRL*** results in a less favorable reaction, by $\Delta\Delta G^\circ$ = +3.5 kcal/mol, due to an unfavorable differential enthalpy ($\Delta\Delta H$ = 12.6 kcal/mol) and favorable differential entropy contributions ($\Delta(T\Delta S)$ = +9.1 kcal/mol).

In the targeting of a RNA structure, relative to its counterpart DNA, it is important to consider the stability of the RNA molecule. For example, in the case of ***rSRL*** and ***dSRL*****,** the RNA is thermodynamically more stable than its DNA analog, by 5.4 kcal/mol, which makes disrupting this structure more dificulty, resulting in a targeting reaction with a less favorable free energy term, by 3.5 kcal/mol. These results show that all DNA targeting reactions can be used to determine the stability of RNA/DNA reaction products, which can be useful in designing complementary strands for the control gene expression provide that both molecules have similar secondary structures and no tertiary structures are involved.

Table 2: Thermodynamic Profiles for Targeting Reactions.

	Transition	T_M (°C)	ΔH (kcal/mol)	$T\Delta S$ (kcal/mol)	$\Delta G^\circ_{(5)}$(kcal/mol)
Reaction One					
rSRL	1	61.0	48.3	40.2	8.1
	2	69.1	41.6	33.8	7.8
			89.9	**74.0**	**15.9**
CS	1	32.3	6.8	6.2	0.6
	2	43.8	11.7	10.3	1.4
			18.5	**16.5**	**2.0**
Hybrid-Duplex	1	63.9	43.6	36.0	7.6
	2	70.5	104	84.2	19.8
			147.6	**120.2**	**27.4**
Reaction Two					
dSRL	1	54.8	**69.1**	**58.6**	**10.5**
DNA-Duplex	1	63.4	34.4	28.4	6.0
	2	68.5	105	85.5	19.5
			139.4	**113.9**	**25.5**
Hess Cycle					
Reaction One			**39.2**	**29.7**	**9.5**
Reaction Two			**51.8**	**38.8**	**13.0**

All experiments were done in 10 mM sodium phosphate buffer and 100 mM NaCl at pH 7.0. Experimental errors are as follows: T_M (± 0.5 °C), ΔH (± 5 %), $T\Delta S$ (± 5 %), $\Delta G^\circ_{(5)}$ (± 7%), ΔH_{HC} (± 10 %), $T\Delta S_{HC}$ (± 10 %), ΔG°_{HC} (± 14%). Thermodynamic profiles for the unfolding of the complementary strand is included.

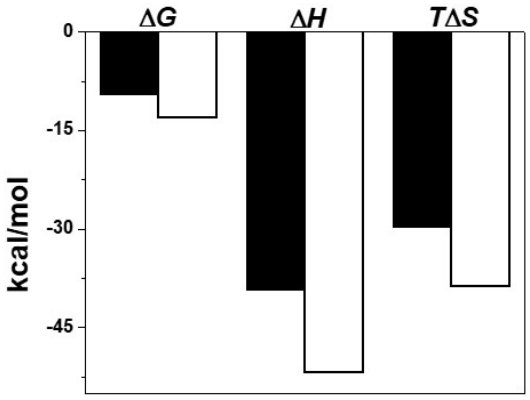

Figure 6: Comparison of targeting thermodynamics: ***rSRL*** (solid bars) and ***dSRL*** targeting (open bars) $\Delta\Delta G$ = +3.5, $\Delta\Delta H$ = +12.6 and $\Delta(T\Delta S)$= + 9.1

4. Conclusion

We have investigated the thermodynamic stability of the Sarcin Ricin Loop and its DNA analog to determine the differences in their formation and stability. Specifically, we used a combination of UV and DSC to determine the unfolding thermodynamics of ***rSRL*** and ***dSRL*** and their reaction with a DNA complementary strand. The favorable folding of both RNA and DNA hairpins results from the typical favorable enthalpy-unfavorable entropy compensation. The unfolding data shows that ***rSRL*** is more stable (by 5.4 kcal/mol) due to a higher thermal stability and a higher enthalpy contribution. The targeting thermodynamic data indicated that the complementary strand is able to disrupt both ***rSRL*** and ***dSRL***. The resulting RNA/DNA and DNA/DNA duplex products show very similar unfolding thermodynamic profiles. However, the disruption of ***rSRL*** takes place with a less favorable free energy contribution (by 3.5 kcal/mol) due to the higher thermodynamic stability of the RNA. Therefore, in the case of the Sarcin Ricin Loop, which forms a hairpin, an all DNA targeting system can be used to obtain information regarding the final RNA/DNA reaction product In practice, the favorable free energy term of targeting reactions may be increased by improving the stability of the duplex products, by using longer single strands with complementary sequences and/or DNA intramolecular structures with loops containing a larger number of unpaired bases. Furthermore, to determine if this particular model system is applicable to more complex structures besides simple hairpins, similar comparison of RNA and DNA molecules with different secondary structures will be needed; especially, with the inclusion of Mg^{2+} ions and osmolytes because of their potential to induce tertiary interactions and to resemble the cellular media, respectively.

5. Acknowledgements

This work was supported by Grants MCB-1122029 and MCB-1912587 from the National Science Foundation, and a GAANN graduate fellowship (C.R.) of Grant P200A120231 from the US Department of Education.

6. References

1. Moazed, D., J.M. Robertson, and H.F. Noller. 1988. Interaction of elongation factors EF-G and EF-Tu with a conserved loop in 23S RNA. Nature. 334: 362–364.

2. Wintermeyer, W., F. Peske, M. Beringer, K.B. Gromadski, a Savelsbergh, and M. V Rodnina. 2004. Mechanisms of elongation on the ribosome: dynamics of a macromolecular machine. Biochem. Soc. Trans. 32: 733–737.

3. Hausner, T.P., J. Atmadja, and K.H. Nierhaus. 1987. Evidence that the G2661 region of 23S rRNA is located at the ribosomal binding sites of both elongation factors. Biochimie. 69: 911–923.

4. Nilsson, J., and P. Nissen. 2005. Elongation factors on the ribosome. Curr. Opin. Struct. Biol. 15: 349–354.

5. Munishkin, a, and I.G. Wool. 1997. The ribosome-in-pieces: binding of elongation factor EF-G to oligoribonucleotides that mimic the sarcin/ricin and thiostrepton domains of 23S ribosomal RNA. Proc. Natl. Acad. Sci. U. S. A. 94: 12280–4.

6. Sergiev, P. V., A.A. Bogdanov, and O.A. Dontsova. 2005. How can elongation factors EF-G and EF-Tu discriminate the functional state of the ribosome using the same binding site? FEBS Lett. 579: 5439–5442.

7. Endo, Y., and I.G. Wool. 1982. The site of action of alpha-sarcin on eukaryotic ribosomes. The sequence at the alpha-sarcin cleavage site in 28 S ribosomal ribonucleic acid. J. Biol. Chem. 257: 9054–9060.

8. Endo, Y., and K. Tsurugi. 1987. RNA N-glycosidase activity of ricin A-chain. Mechanism of action of the toxic lectin ricin on eukaryotic ribosomes. J. Biol. Chem. 262: 8128–8130.

9. Ban, N. 2000. The Complete Atomic Structure of the Large Ribosomal Subunit at 2.4 A Resolution. Science (80-.). 289: 905–920.

10. Wool, I.G., A. Glück, and Y. Endo. 1992. Ribotoxin recognition of ribosomal RNA and a proposal for the mechanism of translocation. Trends Biochem. Sci. 17: 266–269.

11. Szewczak, a a, and P.B. Moore. 1995. The sarcin/ricin loop, a modular RNA. J. Mol. Biol. 247: 81–98.

12. Correll, C.C., a Munishkin, Y.L. Chan, Z. Ren, I.G. Wool, and T. a Steitz. 1998. Crystal structure of the ribosomal RNA domain essential for binding elongation factors. Proc. Natl. Acad. Sci. U. S. A. 95: 13436–13441.

13. Correll, C.C., I.G. Wool, and A. Munishkin. 1999. The two faces of the Escherichia coli 23 S rRNA sarcin/ricin domain: the structure at 1.11 A resolution. J Mol Biol. 292: 275–287.

14. Szewczak, A.A., P.B. Moore, Y.L. Chang, and I.G. Wool. 1993. The conformation of the sarcin/ricin loop from 28S ribosomal RNA. Proc. Natl. Acad. Sci. U. S. A. 90: 9581–5.

15. Ingle, S., R.N. Azad, S.S. Jain, and T.D. Tullius. 2014. Chemical probing of RNA with the hydroxyl radical at single-atom resolution. Nucleic Acids Res. 42: 12758–12767.

16. Correll, C.C., J. Beneken, M.J. Plantinga, M. Lubbers, and Y.L. Chan. 2003. The common and the distinctive features of the bulged-G motif based on a 1.04 A resolution RNA structure. Nucleic Acids Res. 31: 6806–6818.

17. Agrawal, R.K., P. Penczek, R. a Grassucci, and J. Frank. 1998. Visualization of elongation factor G on the Escherichia coli 70S ribosome: The mechanism of translocation. Proc. Natl. Acad. Sci. 95: 6134–6138.

18. Ban, N., P. Nissen, J. Hansen, M. Capel, P.B. Moore, and T. a Steitz. 1999. Placement of protein and RNA structures into a five A-resolution map of the 50S ribosomal subunit. Nature. 400: 841–847.

19. Saxena, S.K., and E.J. Ackerman. 1990. Microinjected oligonucleotides complementary to the α-sarcin loop of 28 S RNA abolish protein synthesis in Xenopus oocytes. J. Biol. Chem. 265: 3263–3269.

20. Crooke, S.T. 1999. Molecular mechanisms of action of antisense drugs. Biochim. Biophys. Acta - Gene Struct. Expr. 1489: 31–43.

21. Hélène, C. 1991. Rational design of sequence-specific oncogene inhibitors based on antisense and antigene oligonucleotides. Eur. J. Cancer Clin. Oncol. 27: 1466–1471.

22. Beal, P.A., and P.B. Dervan. 1991. Second structural motif for recognition of DNA by oligonucleotide- directed triple-helix formation. Science (80-.). 251: 1360–1363.

23. Brown, P.M., C.A. Madden, and K.R. Fox. 1998. Triple-helix formation at different positions on nucleosomal DNA. Biochemistry. 37: 16139–16151.

24. Lee, H.T., C.M. Olsen, L. Waters, H. Sukup, and L.A. Marky. 2008. Thermodynamic contributions of the reactions of DNA intramolecular structures with their complementary strands. Biochimie. 90: 1052–1063.

25. Prislan, I., H.T. Lee, C. Lee, and L.A. Marky. 2015. The size of the internal loop in DNA hairpins influences their targeting with partially complementary strands. J. Phys. Chem. B. 119: 96–104.

26. Lee, H.T., C. Carr, H. Siebler, L. Waters, I. Khutsishvili, F. Iseka, B. Domack, C.M. Olsen, and L.A. Marky. 2011. A thermodynamic approach for the targeting of nucleic acid structures using their complementary single strands. Methods Enzymol. 492: 1–26.

27. Reiling, C., and L.A. Marky. 2014. Contributions of the loops on the stability and targeting of DNA pseudoknots. Biochem. Compd. 2.

28. Cantor, C.R., M.M. Warshaw, and H. Shapiro. 1970. Oligonucleotide interactions. III. Circular dichroism studies of the conformation of deoxyoligonucleolides. Biopolymers. 9: 1059–1077.

29. Borer, P. 1975. Optical properties of nucleic acids, absorption and circular dichroism spectra. In: G.D. Fasman, editor. CRC Handbook of Biochemistry and Molecular Biology: Nucleic Acids. Boca Raon, FL: . pp. 589–595.

30. Marky, L.A., S. Maiti, C. Olsen, R. Shikiya, S.E. Johnson, M. Kaushik, and I. Khutsishvili. 2007. Building Blocks of Nucleic Acid Nanostructures: Unfolding Thermodynamics of Intramolecular DNA Complexes. In: Biomedical Applications of Nanotechnology. John Wiley & Sons, Inc. pp. 191–226.

31. Marky, L.A., and K.J. Breslauer. 1987. Calculating thermodynamic data for transitions of any molecularity from equilibrium melting curves. Biopolymers. 26: 1601–1620.

32. Rentzeperis, D., J. Ho, and L.A. Marky. 1993. Contribution of Loops and Nicks to the Formation of DNA Dumbbells: Melting Behavior and Ligand Binding. Biochemistry. 32: 2564–2572.

33. 3Erie, D., W. Olson, R. Jones, K. Breslauer, and N. Sinha. 1987. A Dumbbell-Shaped, Double-Hairpin Structure of DNA: A Thermodynamic Investigation. Biochemistry. 26: 7150–7159.

34. Xia, T., J. SantaLucia, M.E. Burkard, R. Kierzek, S.J. Schroeder, X. Jiao, C. Cox, and D.H. Turner. 1998. Thermodynamic parameters for an expanded nearest-neighbor model for formation of RNA duplexes with Watson - Crick base pairs. Biochemistry. 37: 14719–14735.

35. SantaLucia, J. 1998. A unified view of polymer, dumbbell, and oligonucleotide DNA nearest-neighbor thermodynamics. Proc. Natl. Acad. Sci. 95: 1460–1465.

36. Kankia, B.I., and L.A. Marky. 1999. DNA, RNA, and DNA/RNA Oligomer Duplexes: A Comparative Study of Their Stability, Heat, Hydration, and Mg 2+ Binding Properties. J. Phys. Chem. B. 103: 8759–8767.

37. Saenger, W. 1984. Principles of Nucleic Acid Structure. .

38. Auffinger, P., and E. Westhof. 1999. Roles of Hydration on the Structure and Dynamics of Nucleic Acids. In: Ross TH, RB Leslie, PJ Lillford, editors. Water Management in the Design and Distribution of Quality Foods. Technomic

Publishing Co Inc. pp. 165–198.

39. Sugimoto, N., S. Nakano, M. Katoh, and A. Matsumura. 1995. Thermodynamic parameters to predict stability of RNA/DNA hybrid duplexes. Biochemistry. 34: 11211–11216.